Absolute wavelength measurement of the Lyman-α transition of hydrogen-like silicon

J. Tschischgale, D. Klöpfel, P. Beiersdorfer, G.V. Brown, E. Förster, H. Schulte-Schrepping, and S.B. Utter

Abstract: The wavelengths of the $1s_{1/2}$–$2p_{1/2}$ and $1s_{1/2}$–$2p_{3/2}$ Lyman-α transitions have been measured in hydrogenic silicon with an accuracy of 70 ppm. The measurement was carried out with an electron-beam ion trap with a calibrated double-faced monolithic crystal that enabled absolute measurements of the transition wavelengths. The values for the Lyman-α wavelengths are $\lambda_{\mathrm{Ly}\alpha 1} = 6.180\,49(44)$ Å and $\lambda_{\mathrm{Ly}\alpha 2} = 6.185\,56(66)$ Å. The wavelengths are in good agreement with calculations and allow a determination of the $1s$ Lamb shift to within 28% in a region that has received little experimental attention.

PACS Nos.: 32.30Rj, 31.30Jv

Résumé : Nous avons mesuré avec une précision de 70 ppm les longueurs d'onde des transitions Lyman-α, $1s_{1/2}$–$2p_{1/2}$ et $1s_{1/2}$–$2p_{3/2}$, dans du silicium de type hydrogène (Si^{+13}). La mesure utilisait un piège ionique à faisceau d'électrons avec un monocristal à deux faces calibrées permettant des mesures absolues des longueurs d'onde des transitions. Les valeurs obtenues sont $\lambda_{\mathrm{Ly}\alpha 1} = 6{,}180\,49(44)$ Å et $\lambda_{\mathrm{Ly}\alpha 2} = 6{,}185\,56(66)$ Å. Les longueurs d'onde sont en bon accord avec les valeurs calculées et permettent de déterminer le déplacement de Lamb à 28 % près dans une région qui a été peu explorée expérimentalement.

[Traduit par la Rédaction]

1. Introduction

Precision measurements of the Lyman-α wavelengths allow the determination of the so-called Lamb shift. The Lamb shift, discovered by Lamb and Retherford [1] and first explained by Bethe [2], is the sum of nuclear size effects and contributions from quantum electrodynamics (QED). It scales as $(\alpha Z)^4/n^3$, where α is the fine-structure constant, Z is the atomic number, and n is the principal quantum number. As a consequence, the shift is largest for transitions involving the $1s$ level [3].

Received 8 May 2002. Accepted 10 May 2002. Published on the NRC Research Press Web site at `http://cjp.nrc.ca/` on 17 July 2002.

J. Tschischgale,[1] D. Klöpfel, and E. Förster. X-Ray Optics Group, Institute of Optics and Quantum Electronics, Friedrich-Schiller University Jena, Max-Wien Platz 1, D–07743 Jena, Germany.
P. Beiersdorfer,[2] G.V. Brown, and S.B. Utter. Department of Physics and Advanced Technologies, Lawrence Livermore National Laboratory, Livermore, CA 94550, U.S.A.
H. Schulte-Schrepping. HASYLAB, DESY, Notkestraße 85, D–22603 Hamburg, Germany.

[1] Present Address: Carl Zeiss Company, Oberkochen, Germany.
[2] Corresponding author (e-mail: beiersdorfer@llnl.gov).

 DOI: 10.1139/P02-011

Measurements that determined the size of the Lamb shift of the $2p \rightarrow 1s$ (Lyman-α) transitions have been performed for a great number of hydrogen-like ions [4]. Most of these were made at heavy accelerators, focussing on high-Z ions. Between He^{+} and Ar^{17+}, i.e., elements for which the Lamb shift accounts for less than 1 eV of the $2p \rightarrow 1s$ transition energy, only few measurements have been made. In fact, until recently [5], there were no measurements of the Lamb shift of the $2p \rightarrow 1s$ transitions in highly charged ions below sulfur ($Z = 16$).

The Lyman-α transitions of hydrogen-like ions with atomic number below sulfur fall in the soft-X-ray region and have wavelengths above 5 Å. Accurate measurements of such soft-X-ray transitions are now possible by combining several techniques developed during the past few years. These include the use of the electron-beam ion trap for precision QED studies [6–8], the implementation of high-resolution soft-X-ray spectrometers [9], and the development of absolutely calibrated crystals with an appropriately large lattice spacing [10]. This combination of techniques was applied successfully to a measurement of the Lamb shift of the Lyman-α transitions in hydrogen-like Mg^{11+} [5]. The use of a calibrated crystal means that the measurement can be carried out without resorting to external calibration standards during the measurement. This eliminates systematic errors introduced by geometrical effects, i.e., problems caused by the fact that external calibration sources fill the X-ray optics differently than X rays from the ions in the trap, which can greatly complicate the analysis and may lead to unknown systematic errors [11, 12].

In the following, we present a measurement of the silicon Lyman-$\alpha_{1,2}$ transitions ($2p_{3/2} \rightarrow 1s_{1/2}$, $2p_{1/2} \rightarrow 1s_{1/2}$). The measurement was carried out at the Lawrence Livermore National Laboratory (LLNL) electron-beam ion trap (EBIT–II), which is the second such device constructed. Unlike the earlier measurement of Mg^{11+}, which employed two separate, small, optically coupled crystals, the present measurement utilizes a large, monolithic crystal with two reflecting faces cut from a single block of material.

The Lamb-shift contribution to the two silicon Lyman-α transitions was calculated by Johnson and Soff [13] to be 0.48 eV. This is 0.026% of the total transition energy. The present measurement tests this prediction within 28%.

2. Experimental setup

A detailed description of the physical properties of the Livermore electron-beam ion trap used to produce hydrogen-like silicon ions was given in refs. 14 and 15. Silicon was injected using a metal vapor vacuum arc (MeVVA) [16], which sputtered ions out of a silicon–magnesium alloy. The silicon ions were generated by electron impact ionization, which could be controlled by the electron-beam energy. X rays radiated from excited ions were observed through radial ports.

EBIT–II provides a stationary, Doppler-free line source with a diameter of less than 70 μm. The ion temperature has been estimated to be about 300 eV [9] for the present conditions.

The measurement was performed with a vacuum crystal spectrometer employing a monolithic silicon crystal with the reflex (111). The dimensions of the crystal were 53 mm (length) by 45 mm (width) by 39 mm (height). As described in ref. 10, the main idea behind using a monolithic crystal was based on a proposal by Uhler and Cooksey [17–19] to determine wavelengths without the need of a calibration source. This idea was improved by Förster et al. [20, 21] by replacing the shift of the detector with a displacement of crystal planes of a double-faced monolith, which can be measured more precisely. The arrangement used for our measurement is illustrated in Fig. 1. The distance between the crystal surfaces L was measured to be $L = 44.972$ mm with an accuracy of $\Delta L/L = 1.6 \times 10^{-4}$.

To make an absolute wavelength measurement, the lattice spacing of the crystalline layers needs to be calibrated in a comparison with well-known wavelength standards. This was done in a three-step process. First, the lattice spacing of a reference crystal was calibrated at PTB Braunschweig, Germany, using optic-interferometric and X-ray-interferometric measurements in a comparison to optical wavelength standards [22]. Second, the reference crystal was used to calibrate a Bond diffractometer at the University

Fig. 1. Schematic of the monolith setup: (*a*) side view, (*b*) top view. The Bragg reflection of a source *S* at the front and at the back surface of the monolith results in two images on the detector separated by the distance *a*.

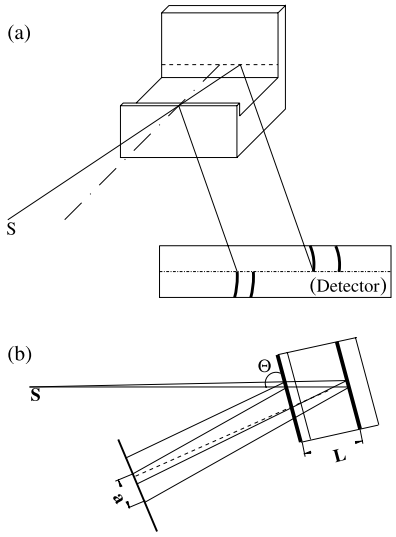

of Jena, Germany [23, 24]. The determination of the lattice spacing was done in step three, using the same Bond diffractometer. With this procedure, the lattice spacing d was measured absolutely in SI units with an accuracy better then 1 ppm, i.e., $d = 3.13\,557\,79$ Å with an accuracy of $\Delta d/d = 9.6 \times 10^{-7}$.

X-rays coming from the line source are reflected at the front and back face of the monolith. As a result, one can see two almost identical spectra on the detector, whose separation a depends only on d, L, the angle between the detector and the crystal surface ζ, and the Bragg angle Θ. Generalizing the expressions given in refs. 10 and 5 to include ζ the dependence of the Bragg angle on the geometrical properties becomes

$$\sin(\Theta) = \frac{2L + a\sin(\zeta)}{\sqrt{4L^2 + 4La\sin(\zeta) + a^2}} \tag{1}$$

This angle cannot be used directly with Bragg's law to determine a wavelength, since the refractive index of the crystal differs slightly from the one in vacuum and depends on the X-ray wavelength.

Crystals have the property of being less dense than a vacuum for X-rays. The index of refraction n can be written as

$$n = 1 - \delta(\lambda) \tag{2}$$

where $\delta(\lambda)$ is the wavelength-dependent deviation from unity and is of the order of 10^{-4}. The measured wavelength can be expressed with the correction of the refractive index and (1) in a Taylor series of δ as

$$\lambda = 2d \times \left(\sin(\Theta) - \frac{\delta}{\sin(\Theta)}\right) \tag{3}$$

$\delta(\lambda)$ was calculated for many of the elements by Henke et al. [25] and can be expressed in the energy range of the silicon Lyman-α doublet ($\lambda \sim 6.18$ Å) as

$$\delta(\lambda) = \delta_0 + \lambda \times \delta_1 \tag{4}$$

where $\delta_0 = 3.367\,96 \times 10^{-5}$ and $\delta_1 = 1.126\,93 \times 10^{-5}$ Å.

Fig. 2. Spectrum of silicon Lyman-$\alpha_{1,2}$ X-ray events on the detector. The difference in relative height can be explained by the absorption of X-rays, reflected by the back face of the crystal, by an aluminum bar in front of the entrance window of the detector.

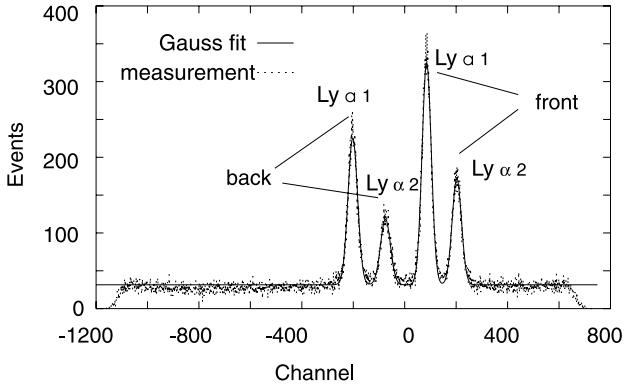

With this, (3) can be solved and an error estimate can be obtained, allowing a selection of parameters to increase the resolution of the setup

$$\left(\frac{\Delta\lambda}{\lambda}\right)_{2d} \simeq \frac{\Delta\, 2d}{2d} \tag{5}$$

$$\left(\frac{\Delta\lambda}{\lambda}\right)_{\delta_1} \simeq \frac{\lambda \times \Delta\delta_1}{\sin^2(\Theta)} \tag{6}$$

$$\left(\frac{\Delta\lambda}{\lambda}\right)_{\delta_0} \simeq \frac{\Delta\delta_0}{\sin(\Theta)} \tag{7}$$

$$\left(\frac{\Delta\lambda}{\lambda}\right)_{\zeta} \simeq \frac{\cos^2(\Theta)}{\cos(\zeta)}\left(\frac{a}{2L} + \sin(\zeta)\right) \times \Delta\zeta \tag{8}$$

$$\left(\frac{\Delta\lambda}{\lambda}\right)_{L} \simeq \cos^2(\Theta) \times \frac{\Delta L}{L} \tag{9}$$

$$\left(\frac{\Delta\lambda}{\lambda}\right)_{a} \simeq \cos^2(\Theta) \times \frac{\Delta a}{a} \tag{10}$$

It can easily be seen that all errors caused by geometry disappear at the Bragg angle $\Theta = 90°$. The errors caused by the refractive index are one order of magnitude smaller than the error of the lattice-spacing measurement.

For the silicon Lyman-α X-rays and our silicon monolith the Bragg angle is about $\Theta \sim 80°$. According to the estimate above, this minimizes all geometrical errors to about 3% of their nominal value.

The spectrometer employed a one-dimensional position sensitive gas proportional counter. Since the determination of wavelengths depends on the separation of the shifted spectra on the detector, the spatial response of the detector had to be calibrated very accurately. The calibration was done with an ^{55}Fe source using a 100 μm slit in front of the detector. The slit was moved with a high-precision micrometer drive to cover the spatial extent of the Lyman-α spectrum in 27 steps each 1 mm apart. The dependence of source position on the channel number of the detector was fitted with a third-order polynomial. A correction for temperature effects was necessary. The calibration was done at an average room temperature T_{R}. The high-precision micrometer drive is made of steel and was calibrated at a temperature of 293 K. During measurement, the temperature of the detector T_{M} was even higher, since

the preamplifier heated up the detector in vacuum because of reduced heat conduction. The detector, made of aluminum, expanded during the measurement. The corrected distance a_k at the temperature of the measurement can be calculated with the linear expansion coefficient of steel α_{st} and aluminum α_{Al}

$$a_k = a \times (1 + \alpha_{\mathrm{Al}}(T_{\mathrm{M}} - T_{\mathrm{R}}) + \alpha_{\mathrm{st}}(T_{\mathrm{R}} - 293\ \mathrm{K})) \tag{11}$$

The correction is on the order of $\Delta a/a = 2 \times 10^{-4}$, which is significant for the results.

Another correction had to be made for the thermal expansion of the lattice spacing d and of the distance L of the crystal. The temperature of the crystal in vacuum was monitored during the experiment. The correction is about $\Delta d/d = \Delta L/L = 7 \times 10^{-6}$.

3. Measurement and analysis

The measurement was done using event mode counting [26], which meant that for every event measured in the detector, the position in the detector, the pulse height of the X-ray signal, and the timing cycle of EBIT were recorded. This allowed uninteresting energy regions and times of the EBIT cycle before ionization starts to be gated out. The resulting spectrum of the silicon Lyman-α transitions is shown in Fig. 2.

The profile of the lines measured on the detector is a convolution of the natural line profile, the finite size of the source, the Doppler broadening, the rocking curve, the spectral aberrations of the spectrometer geometry, and the spatial resolution of the detector. A detailed discussion of these influences was made by Härtwig and Großwig [27].

Because of the influence of the spectral aberration and the rocking curve, which can be described as a Lorentzian [28], the line profile on the detector is expected to be a Lorentz profile. The Gauss-shaped broadening of the lines caused by the detector resolution is estimated to be much smaller than these effects. Contributions resulting from the source dimensions are negligibly small.

In contrast to this expectation, the best-fit function is a Gauss profile. The fit was done using a weighted Levenberg–Marquardt method to determine the peak position. The fact that a Gauss profile provides the best fit to the data shows that Doppler broadening is the dominant line-broadening mechanism. A line width of 0.65 eV is determined. The deconvolution with the known rocking curve of the crystal leads to a contribution of 0.52 eV from Doppler broadening. This corresponds to an ion temperature of 304 eV, which is reasonable when compared with the ion temperature measured on EBIT–II before [9, 29].

Table 1 shows the errors of the measurement. The final wavelengths of the silicon Lyman-$\alpha_{1,2}$ transition were determined to be 6.180 49(44) Å for Lyman-α_1 and 6.185 56(66) Å for Lyman-α_2. This compares to 6.180 43 Å and 6.185 84 Å, respectively, calculated in ref. 13.

4. Discussion

Together with the earlier mesurements of Mg^{11+} the present measurements show that the soft-X-ray region is amenable to measurements that are absolutely calibrated. An arrangement with external calibration sources is not necessary, avoiding hard to assess systematic errors, such as those described by Chantler et al. in measurements of hydgrogen-like V^{22+} and helium-like V^{21+} [11, 12], caused by the fact that external X-ray sources illuminate the X-ray optics differently than the X rays from the trapped ions.

The contributions to the Lamb shift can be calculated by subtracting the Dirac eigenvalue for a point nucleus [13] from the transition energy. The results are $4028 \pm 1132\ \mathrm{cm}^{-1}$ for Lyman-α_1 and $3167 \pm 1616\ \mathrm{cm}^{-1}$ for Lyman-α_2. This compares with $3577\ \mathrm{cm}^{-1}$ and $3892\ \mathrm{cm}^{-1}$ calculated in ref. 13. A graphical comparison is shown in Fig. 3. Similar to the values measured for the neighboring elements, the present values are in good agreement with the values calculated by Johnson and Soff [13].

Table 1. Contributions to the measurement uncertainties. The main uncertainty results from determining the separation of the lines on the detector. 85% of this uncertainty is from the fit and 15% is from the detector calibration.

	Lyman-α_1	Lyman-α_2
$\frac{\Delta\lambda}{\lambda}(2d)$	9.6×10^{-7}	9.6×10^{-7}
$\frac{\Delta\lambda}{\lambda}(\delta_1)$	2.9×10^{-8}	2.9×10^{-8}
$\frac{\Delta\lambda}{\lambda}(\delta_0)$	2.9×10^{-8}	2.9×10^{-8}
$\frac{\Delta\lambda}{\lambda}(L)$	4.6×10^{-6}	4.3×10^{-6}
$\frac{\Delta\lambda}{\lambda}(a)$	6.0×10^{-5}	9.4×10^{-5}
$\frac{\Delta\lambda}{\lambda}(T)$	4.0×10^{-6}	4.0×10^{-6}
$\frac{\Delta\lambda}{\lambda}(\zeta)$	1.8×10^{-6}	4.6×10^{-6}
$\sum$	7.0×10^{-5}	1.0×10^{-4}

Fig. 3. Comparison of measured and calculated Lamb-shift contributions: (*a*) Lyman-α_1 and (*b*) Lyman-α_2. Theoretical values (conntinuous lines) are from ref. 13. Values for Si^{13+} are present measurements. The data for Mg^{11+} are from ref. 5, for S^{15+} are from ref. 33, for Cl^{16+} are from refs. 34–36, and for Ar^{17+} are from refs. 37–39. Error bars represent one-sigma confidence limits.

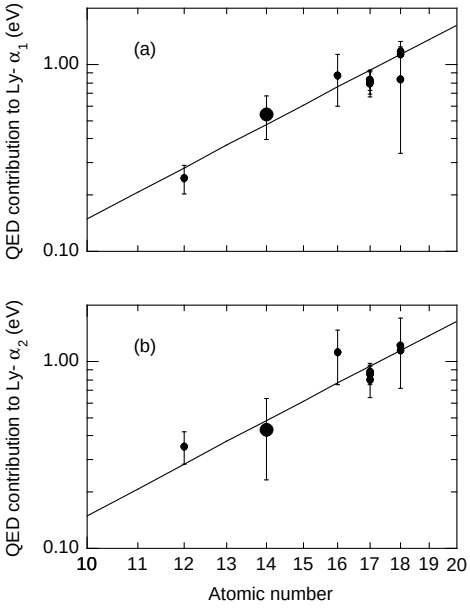

The development of accurate wavelength measurements of soft-X-ray transitions may also benefit Lamb-shift determinations of transitions in ions with very high atomic numbers. Several $2p_{3/2} \rightarrow 2s_{1/2}$ transitions in lithium-like ions (Ir^{74+}, for example) fall in the same wavelength band as Mg^{11+} or Si^{13+}. These transitions are strongly affected by QED [30]. In fact, the QED contributions are much higher than those of the Lyman transitions in this wavelength band, making them very interesting for testing atomic theory [31, 32]. The present results show that absolute measurements of these transitions are possible provided similar X-ray count rates as in the present measurement can be achieved.

Acknowledgments

This work was supported in part by the Department of Energy, Office of Basic Energy Sciences, and an International Collaboration grant from the Deutscher Akademischer Austauschdienst and was performed by the University of California Lawrence Livermore National Laboratory under the auspices of the Department of Energy under contract No. W-7405-ENG-48.

References

1. W.E. Lamb and R.C. Retherford. Phys. Rev. **72**, 241 (1947).
2. H.A. Bethe. Phys. Rev. **72**, 339 (1947).
3. G. Soff, I. Bednyakov, T. Beier, F. Erler, I.A. Goidenko, U.D. Jentschura, L.N. Labzowsky, A.V. Nefiodov, G. Plunien, R. Schützhold, and S. Zschocke. Hyperfine Int. **132**, 75 (2001).
4. H.F. Beyer, H.J. Kluge, and V.P. Shevelko. X-ray radiation of highly charged ion. Springer Verlag, Berlin. 1997.
5. G. Hölzer, E. Förster, D. Klöpfel, P. Beiersdorfer, G. Brown, J.R. Crespo López-Urrutia, and K. Widmann. Phys. Rev. A: At. Mol. Opt. Phys. **57**, 945 (1998).
6. P. Beiersdorfer, M.H. Chen, R.E. Marrs, and M.A. Levine. Phys. Rev. A, **41**, 3453 (1990).
7. P. Beiersdorfer, D. Knapp, R.E. Marrs, S.R. Elliott, and M.H. Chen. Phys. Rev. Lett. **71**, 3939 (1993).
8. P. Beiersdorfer, A. Osterheld, J. Scofield, J. Crespo López-Urrutia, and K. Widmann. Phys. Rev. Lett. **80**, 3022 (1998).
9. P. Beiersdorfer, J.R. Crespo López-Urrutia, E. Förster, J. Mahiri, and K. Widmann. Rev. Sci. Instrum. **68**, 1077 (1996).
10. D. Klöpfel, G. Hölzer, E. Förster, and P. Beiersdorfer. Rev. Sci. Instrum. **68**, 3669 (1997).
11. C.T. Chantler, D.J. Paterson, L.T. Hudson, F.G. Serpa, J.D. Gillaspy, and E. Takács. Phys. Scr. **T80**, 440 (1999).
12. C.T. Chantler, D. Paterson, L.T. Hudson, F.G. Serpa, J.D. Gillaspy, and E. Takács. Phys. Rev. A: At. Mol. Opt. Phys. **62**, 042501 (2000).
13. W.R. Johnson and G. Soff. At. Data and Nucl. Data Tables, **33**, 405 (1985).
14. M.A. Levine, R.E. Marrs, J.R. Henderson, D.A. Knapp, and M.B. Schneider. Phys. Scr. **22**, 157 (1988).
15. R.E. Marrs, P. Beiersdorfer, and D. Schneider. Phys. Today, **472**, Oct. 27 (1994).
16. I.G. Brown, J.E. Galvin, R.A. MacGill, and R.T. Wright. Appl. Phys. Lett. **49**, 1019 (1986).
17. H.S. Uhler and C.D. Cooksey. Phys. Rev. **10**, 645 (1917).
18. H.S. Uhler. Phys. Rev. **11**, 1 (1918).
19. C.D. Cooksey and D. Cooksey. Phys. Rev. **36**, 85 (1930).
20. E. Förster, K. Goetz, S. Großwig, K. Schäfer, W.D. Zimmer, and K. Sander. Preprint Univ. Jena, **N/83/38** (1983).
21. A.V. Rode, A.M. Maksimchuk, G.V. Sklizkov et al. J. X-Ray Sci. Technol. **2**, 149 (1990).
22. P. Becker, K. Dorenwendt, G. Ebeling et al. Phys. Rev. Lett. **46**, 1540 (1981).
23. W.L. Bond. Acta Crystallogr. **13**, 814 (1960).
24. S. Großwig, J. Härtwig, H.-J. Jäckel, R. Kittner, and W. Melle. Sci. Instrum. **1**, 29 (1986).
25. B.L. Henke, E.M. Gullikson, and J.C. Davis. At. Data Nucl. Data Tables, **54**, 181 (1993).
26. P. Beiersdorfer, G.V. Brown, L. Hildebrandt, K. Wong, and R. Ali. Rev. Sci. Instrum. **72**, 508 (2001).
27. J. Härtwig and S. Großwig. Phys. Scr. **115**, 369 (1989).
28. B.L. Henke. J. Appl. Phys. **49**, 480 (1978).
29. P. Beiersdorfer, V. Decaux, S.R. Elliott, K. Widmann, and K. Wong. Rev. Sci. Instrum. **66**, 303 (1995).
30. Y.-K. Kim, D.H. Baik, P. Indelicato, and J.P. Desclaux. Phys. Rev. A, **44**, 148 (1991).
31. D.K. McKenzie and G.W.F. Drake. Phys. Rev. A, **44**, R6973 (1991).
32. J. Sapirstein and K.T. Cheng. Phys. Rev. A: At. Mol. Opt. Phys. **64**, 022502 (2001).
33. L. Schleinkofer, F. Bell, H.D. Betz, G. Trollmann, and J. Rothermel. Phys. Scr. **25**, 917 (1982).
34. P. Richard, M. Stockli, R.D. Deslattes, R. Cowan, R.E. LaVilla, B. Johnson, K. Jones, M. Meron, R. Mann, and K. Schartner. Phys. Rev. A: Gen. Phys. **29**, 2939 (1984).
35. E. Källne, J. Källne, P. Richard, and M. Stöckli. J. Phys. B: At. Mol. Opt. Phys. **17**, L115 (1984).
36. R.D. Deslattes, R. Schuch, and E. Justiniano. Phys. Rev. A: Gen. Phys. **32**, 1911 (1985).

37. J.P. Briand, J.P. Mosse, P. Indelicato, P. Chevallier, D. Girard-Vernhet, A. Chetioui, M.T. Ramos, and J.P. Desclaux. Phys. Rev. A: Gen. Phys. **28**, 1413 (1983).
38. H.F. Beyer, R.D. Deslattes, F. Folkmann, and R.E. LaVilla. J. Phys. B: At. Mol. Opt. Phys. **18**, 207 (1985).
39. E.S. Marmar, J.E. Rice, E. Källne, J. Källne, and R.E. LaVilla. Phys. Rev. A: Gen. Phys. **33**, 774 (1986).